RESEARCH ARTICLE

Spatiotemporal and spectral dynamics of multi-item working memory as revealed by the *n*-back task using MEG

Lars Costers[1] | Jeroen Van Schependom[1,2,3] | Jorne Laton[1,4] |
Johan Baijot[1] | Martin Sjøgård[5] | Vincent Wens[5,6] | Xavier De Tiège[5,6] |
Serge Goldman[5,6] | Miguel D'Haeseleer[1,7] | Marie Beatrice D'hooghe[1,7] |
Mark Woolrich[8,9] | Guy Nagels[1,10,11]

[1]Center For Neurosciences, Vrije Universiteit Brussel, Brussels, Belgium

[2]Departement of Electronics and Informatics (ETRO), Vrije Universiteit Brussel, Brussels, Belgium

[3]Radiology, Universitair Ziekenhuis Brussel, Brussels, Belgium

[4]Institute of Biomedical Engineering (IBME), University of Oxford, Oxford, UK

[5]Laboratoire de Cartographie Fonctionnelle du Cerveau (LCFC), Université Libre de Bruxelles, Brussels, Belgium

[6]Magnetoencephalography Unit, CUB-Hôpital Erasme, Brussels, Belgium

[7]Neurology, National MS Center Melsbroek, Melsbroek, Belgium

[8]Oxford Centre for Human Brain Activity (OHBA), University of Oxford, Oxford, UK

[9]Oxford University Centre for Functional MRI of the Brain (FMRIB), University of Oxford, Oxford, UK

[10]St Edmund Hall, University of Oxford, Oxford, UK

[11]Neurology, Universitair Ziekenhuis Brussel, Brussels, Belgium

Correspondence
Lars Costers, Center For Neurosciences, Vrije Universiteit Brussel, Pleinlaan 2, Brussel 1050, Belgium.
Email: lars.costers@vub.be;

Abstract

Multi-item working memory (WM) is a complex cognitive function thought to arise from specific frequency band oscillations and their interactions. While some theories and consistent findings have been established, there is still a lot of unclarity about the sources, temporal dynamics, and roles of event-related fields (ERFs) and theta, alpha, and beta oscillations during WM activity. In this study, we performed an extensive whole-brain ERF and time-frequency analysis on *n*-back magnetoencephalography data from 38 healthy controls. We identified the previously unknown sources of the *n*-back M300, the right inferior temporal and parahippocampal gyrus and left inferior temporal gyrus, and frontal theta power increase, the orbitofrontal cortex. We shed new light on the role of the precuneus during *n*-back activity, based on an early ERF and theta power increase, and suggest it to be a crucial link between lower-level and higher-level information processing. In addition, we provide strong evidence for the central role of the hippocampus in multi-item WM behavior through the dynamics of theta and alpha oscillatory changes. Almost simultaneous alpha power decreases observed in the hippocampus and occipital fusiform gyri, regions known to be involved in letter processing, suggest that these regions together enable letter recognition, encoding and storage in WM. In summary, this study offers an extensive investigation into the spatial, temporal, and spectral characteristics of *n*-back multi-item WM activity.

KEYWORDS

hippocampus, magnetoencephalography, *n*-back, precuneus, working memory

1 | INTRODUCTION

Multi-item working memory (WM) is an important cognitive function that is frequently used in everyday life. It requires a complex interaction between different cognitive functions such as stimulus encoding, storage, retrieval, replacement, and manipulation. The n-back task is one of the most frequently used paradigms to study multi-item WM in cognitive neuroscience. During the n-back task, a subject is asked to respond by button-press to stimuli in a sequence if the current stimulus corresponds to the nth previous stimulus, with n typically being 1, 2, or 3 (Kirchner, 1958). Different variants of the task exist using visual, verbal, and even olfactory stimuli. In most studies, a 0-back or baseline condition is added where subjects need to respond if a stimulus is equal to a predefined item.

Thanks to electroencephalography (EEG) and a small number of magnetoencephalography (MEG) studies, we have gained a notion of what happens in the brain during multi-item WM. A consistently found event-related potential during the n-back task is a P300 over central–parietal electrodes (for a review see Kok, 2001). In some studies the amplitude of this P300 decreased with increasing WM load (Covey, Shucard, & Shucard, 2017; Dong, Reder, Yao, Liu, & Chen, 2015). In context of the interpretation of this P300 response it is important to note that it is also present in the 0-back condition, supporting the idea that it is primarily a process of stimulus evaluation (Donchin, Ritter, & McCallum, 1978). However, the source of this n-back P300 response or its MEG equivalent, the M300 event-related field (ERF), has not yet been identified.

Another consistent finding during multi-item WM activity is an increase in power in the theta band that increases with WM load in frontal areas (Brookes et al., 2011; Dong et al., 2015; Gevins et al., 1998; Gevins, Smith, McEvoy, & Yu, 1997; Lei & Roetting, 2011). This theta power increase has been found to be more robustly elicited in the n-back task than in the delayed-match-to-sample (DMS) task, another popular multi-item WM task (Brookes et al., 2011). A decrease in power relative to baseline or desynchronization has been repeatedly observed in the alpha (Chen & Huang, 2016; Dong et al., 2015; Gevins et al., 1997, 1998; Lei & Roetting, 2011) and beta band (Bočková, Chládek, Jurák, Halámek, & Rektor, 2007; Brookes et al., 2011; Krause, Pesonen, & Hämäläinen, 2010; Pesonen, Hämäläinen, & Krause, 2007), with this power decrease also growing with WM load. Interestingly, two studies found an increase in beta band power with increasing WM load (Chen & Huang, 2016; Deiber et al., 2007). The exact sources of these theta, alpha, and beta oscillatory changes during n-back activity are still ill-defined. Gaining insight into those sources could help guiding research and possible new therapies for impaired WM as a consequence of, for example, neurodegenerative disease or traumatic brain injury.

Theta oscillations during general WM brain activity have been thought to serve multiple functions. Studies have suggested a role in sensory gating (Raghavachari et al., 2001), the encoding of temporal information of WM items (Hsieh, Ekstrom, & Ranganath, 2011; Lisman & Idiart, 1995; Lisman & Jensen, 2013; Roberts, Hsieh, & Ranganath, 2013), and the coordination of different sub-functions of WM processes through interregional theta synchronization (for a complete review see Sauseng, Griesmayr, Freunberger, & Klimesch, 2010). Evidence for local generators of WM theta oscillations in humans has been found in the occipital/parietal and temporal cortices (Raghavachari et al., 2006) and hippocampus (N. Axmacher et al., 2010; Van Vugt, Schulze-Bonhage, Litt, Brandt, & Kahana, 2010) using intracranial EEG (iEEG). Using noninvasive neuroimaging techniques such as M/EEG, studies almost uniquely reported frontal theta power increases (Jensen & Tesche, 2002; Kawasaki, Kitajo, & Yamaguchi, 2010; for a review see Roux & Uhlhaas, 2014). In monkeys, a decrease in alpha power showed to correlate with an increase in neural spiking (Haegens, Nácher, Luna, Romo, & Jensen, 2011). This is seen as evidence that alpha power changes can modulate information processing. A MEG study by Bonnefond and Jensen (2012) showed changes in alpha power and phase in anticipation of a distracting stimulus during a WM task. These changes were predictive of WM performance, suggesting that alpha oscillations protect the information that is stored in WM from distractors. Stronger decreases in alpha power were also observed in subjects with poor WM, compared to subjects with good WM (Dong et al., 2015). Alpha power modulations during WM have been reported to also extend over the beta band (Bastos, Loonis, Kornblith, Lundqvist, & Miller, 2018; Palva, Kulashekhar, Hämäläinen, & Palva, 2011; Tallon-Baudry, Bertrand, Peronnet, & Pernier, 1998), so it has been suggested that both frequency bands convey the same inhibitory function. Most studies report posterior, parietal, and occipital sources of alpha/beta oscillations (see Roux & Uhlhaas, 2014 for an overview).

Functional magnetic resonance imaging (fMRI) and iEEG literature have explored the brain regions involved in multi-item WM. fMRI studies have played a large role in identifying the network involved in the multi-item WM processing. In a quantitative meta-analysis of 11 verbal-visual n-back fMRI studies, Owen, McMillan, Laird, and Bullmore (2005), found evidence for the activation of nine regions: the lateral premotor cortex, dorsal cingulate/medial premotor cortex, dorsolateral prefrontal cortex, ventrolateral prefrontal cortex, frontal pole, medial posterior parietal cortex (including the precuneus), inferior parietal lobule, medial and lateral cerebellum, and thalamus. While fMRI is outstanding at identifying the exact sources of brain activity, it does not provide a sense of when or in which stage of WM activity a certain region is involved. Such information would help determine the role of the aforementioned brain regions, which is currently strongly lacking in the literature. Surprisingly, this n-back fMRI meta-analysis did not report any hippocampal activation, while its important role during multi-item WM behavior has been repeatedly confirmed by iEEG studies both in rodents, using hippocampal lesioning (Fortin, Agster, & Eichenbaum, 2002; Kesner, Gilbert, & Barua, 2002), and humans (Axmacher et al., 2010; Axmacher et al., 2007; for review see Leszczynski, 2011).

In conclusion, there are multiple contradictory findings between imaging modalities and there is a lot of unclarity about the exact sources of oscillatory power changes during n-back WM activity. As mentioned before, understanding the complete spatial, temporal, and spectral dynamics of multi-item WM activity and the role of specific brain regions could be of incredible value identifying the causes of impaired WM in clinical populations and help target potential treatments. This study will

perform an ERF and time-frequency analysis using an assumption-free and whole-brain approach that leverages the excellent temporal (<1 ms) and spatial resolution (2–5 mm) (Hari & Salmelin, 2012) of MEG. While the ability of MEG to probe deep brain activity has been heavily discussed, recent studies have repeatedly shown the sensitivity for deep subcortical sources that are relevant for WM activity, such as the hippocampus (Pizzo et al., 2019; for review see Pu, Cheyne, Cornwell, & Johnson, 2018). Overall, this study aims at providing novel insights into the spatial, temporal, and spectral dynamics of neural events occurring during the n-back WM task through the investigation of ERFs and power changes in relevant frequency bands.

2 | METHODS AND MATERIALS

2.1 | Participants

Thirty-eight healthy subjects aged between 18 and 65 years (M = 47.9, SD = 11.9) with normal or corrected vision performed a visual verbal n-back task. Participants were screened for any neurological or physical conditions that could influence the performance or data acquired during the task, and all participants provided written informed consent. Ethical approval for the study was provided by the ethics committees of the National MS Center Melsbroek (2015-02-12) and the University Hospital Brussels (Commissie Medische Ethiek UZ Brussel, B.U.N. 143201423263, 2015/11). The mean education level of participants was 15 years ±2. Of the 38 participants, 15 (39.5%) were male.

2.2 | n-Back task

The task was partitioned into 12 blocks, that is, 4 blocks per n-back condition (0-back, 1-back, 2-back). A total of 240 stimuli (20 per block) were presented with, respectively, 25, 23, and 28 targets for the three conditions. Participants were instructed to press a button with their right hand when the letter that appeared on the screen was the letter X (0-back), the same letter as the one before (1-back) or the same letter as two letters before (2-back). See Figure 1 for an illustration of the paradigm. The size of the stimuli was 6 by 6.5 cm, and these were projected on a screen which was positioned 72 cm from the front of the MEG helmet. The duration of the stimulus presentation was 1 s, with an intertrial interval of 2.8 s. At the start of every block, the instructions for the condition were presented for 15 s. A photodiode was used to measure the onset of the visual stimuli. Subjects were seated at a distance of 72 cm to the front of the MEG helmet. Important to note is the fact that we also included target trials where subjects did not answer. This was done to ensure that we had an equal and adequate amount of trials for all conditions and subjects.

2.3 | Data acquisition

We recorded neuromagnetic activity in 13 participants on an Elekta VectorView™ system, and 25 on an Elekta Neuromag™ TRIUX system
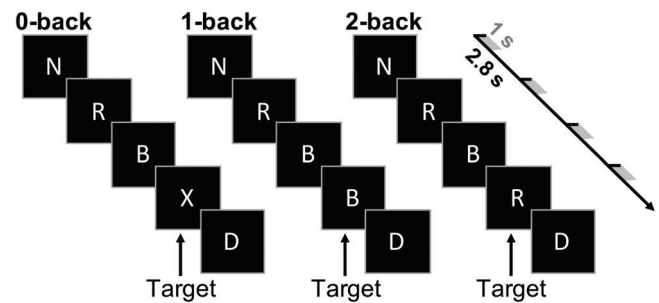

FIGURE 1 Illustration of the visual verbal n-back paradigm. The intertrial interval was 2.8 s and stimuli were presented for 1 s on the screen

(Elekta Oy, Helsinki, Finland), located at the Erasme Hospital (Anderlecht, Belgium). Both are whole-head systems with the exact same sensor layout (306 channels, of which 204 planar gradiometers and 102 magnetometers), and were placed in a light-weight magnetically shielded room (MSR; Maxshield™, MEGIN, Croton Healthcare, Helsinki, Finland) located at the Erasme Hospital (Brussels, Belgium). The characteristics of the MSR have been described elsewhere (De Tiège et al., 2008). The subjects were seated in an upright position with their head positioned to the back of the MEG helmet and were instructed to sit as still as possible during the acquisition. During each recording an electrocardiogram (ECG) and vertical and horizontal electrooculogram (EOG) was recorded for offline artefact rejection. In order to track head movement, four head position indicator coils were attached to the left and right forehead and mastoid. In addition, over 400 points on the scalp and nose were registered using a Polhemus FASTTRAK 3D digitizer (Polhemus, Colchester, VT) together with three fiducials (nasion, left and right preauricular), to obtain the subjects' head shape and allow coregistration with the subject's 3D T1-weighted anatomical magnetic resonance image (MRI). The MRI scan was acquired for all subjects using a 3 Tesla Philips Achieva scanner (Amsterdam, Netherlands) located at the University Hospital Brussels (Jette, Belgium). The data for this study are not publicly available. Researchers interested in a collaboration on these data are welcome to contact the senior authors. Analysis scripts are available upon request from the corresponding author.

2.4 | Data preprocessing and source projection

Data were first preprocessed using the signal-space separation algorithm implemented in the Maxfilter™ software (version 2.2 with default parameters; MEGIN, Croton Healthcare, Helsinki, Finland), using a signal-space separation algorithm to reduce external noise and correct for head movements. All subsequent preprocessing was performed using Oxford's Software Library (OSL; Oxford Centre for Human Brain Activity, UK, https://ohba-analysis.github.io/osl-docs/). This software library uses functions from SPM12 (Welcome Trust Centre for Neuroimaging, University College London) and the Fieldtrip toolbox (Oostenveld, Fries, Maris, & Schoffelen, 2011). Data were

converted to SPM format and downsampled to 250 Hz. Next, independent component analysis with automatic artifactual component rejection was performed using OSL's AFRICA function. Rejections were based on kurtosis (> 20) and correlations with EOG and ECG recordings (> 0.5). The resulting signal and rejected components were manually checked for every subject. Next, data were high-pass filtered at 0.1 Hz, co-registered with individual MRIs, and epoched (see below). We rejected bad channels and trials (median5.82%; IQR) using generalized extreme studentized deviate tests (Rosner, 1983), with a cut-off of significance at .05. We excluded a median of two channels (interquartile range (IQR): [1–6.75]) on a total of 306 channels and 4.89% of the total amount of trials (IQR: [2.66–7.23] %) per subject. Source reconstruction was performed using a bilateral beamformer using Bayesian principal component analysis (Woolrich, Hunt, Groves, & Barnes, 2011). This approach uses a data-driven estimate of the data covariance matrix that automatically trades-off between the signal-to-noise and spatial resolution (Woolrich et al., 2011). A single-shell forward model was used, with a projection on a 5-mm dipole grid. Using an auto-kick detection in the eigenspectra we identified the number of PCs in the data which was reduced after Maxfiltering. Within those PCs the minimum eigenvalue was used to normalize the different sensor types.

2.5 | ERF analysis

Source reconstruction and first-level analysis was performed in OSL. The data were downsampled to 250 Hz and filtered between 0.1 and 40 Hz and epoched from −200 ms to +800 ms relative to stimulus presentation to obtain ERFs. We performed baseline correction on the ERFs using the time period from −200 ms until stimulus presentation, and subject-level and group-level analysis in Fieldtrip.

2.6 | Time-frequency analysis

Source reconstruction and first-level analysis was performed in OSL. Data were downsampled to 250 Hz and initially epoched from −1.2 s to +1.6 s relative to stimulus onset. The fixed intertrial interval was 2.8 s, so there was no overlap of epochs. Time-frequency analysis was performed using the Morlet wavelet method (six cycles) as implemented in Fieldtrip. Because of the high computational demands as consequence of the high spatial resolution of the analyses, we only included three frequencies per band in our analysis. For the theta band, we included 4, 5.5, and 7 Hz. For the alpha band we included 8.5, 10, and 11.5 Hz, and for the beta band 16.5, 21, and 25.5 Hz. Baseline normalization was performed using decibel conversion with a −500 to −100 ms baseline period, after which data was epoched to −200 to +800 ms to remove edge artefacts. Subject-level and group-level analysis were performed in Fieldtrip. Results were averaged within the different frequency bands.

2.7 | Statistics

Source-level ERFs and time-frequency data were converted in statistical spatiotemporal maps. Within each condition (0-back, 1-back, 2-back) and frequency band for time-frequency analyses, single-group t-statistics were calculated for detecting deviations from zero at every point in time and space. For differences between conditions, dependent-sample t-statistics were calculated. We corrected for multiple comparisons by maximum t-statistic (MaxT) testing (Nichols & Holmes, 2002) over time (250 timepoints) and space (14,641 5 mm^3 voxels) with Fieldtrip. The test was performed non-parametrically with permutations (ERF: 2,000, time-frequency: 1,000) and an alpha level of .05 (ERF and theta time-frequency analysis) or .01 (alpha and beta time-frequency analysis). For every permutation of the single-group analyses, a dependent-sample t-test was performed between the participants' data and zero values. When randomly permuting the group labels this corresponds to a sign flipping procedure, which is not implemented in Fieldtrip. For every permutation in the dependent-sample tests, the sample labels of the data from different conditions were randomly permuted. The maximum t-statistic over the whole space × time window for every permutation was taken to construct a permutation H_0 distribution. By comparing the observed t-statistics with this distribution of the H_0 distribution, we obtained a corrected p-value for every space × time point. All reported p-values for the ERF and time-frequency analyses are MaxT-corrected p-values. In order to reduce the large dimensionality and complexity of the results, the thresholded statistical maps were manually scanned for local maxima over the complete time and space dimension. We chose to focus on local maxima instead of looking at the shape or general location of a collection of significant voxels in order to avoid making incorrect conclusions due to source leakage. The anatomical labels for the local maxima of t-maps were chosen based on the Harvard-Oxford Structural atlas. Labels for regions in the sensorimotor network (SMN) were combined as SMN in order to simplify discussion. Because we did not compare groups with differences in scanner type, we did not correct for the type of scanner.

3 | RESULTS

3.1 | Behavioral data

The median reaction time (RT) for the 0, 1, and 2-back condition were, respectively, 446.86 ms (IQR: [398.0–529.3] ms), 457.8 ms (IQR: [392.4–524.2] ms), and 542.7 ms (IQR: [455.4, 608.3] ms). A paired Wilcoxon signed rank test showed a significant difference between the 1-back and 0-back ($Z = −2.15$, $p = .03$), 2-back and 1-back ($Z = −4.43$, $p = 1.41e−5$), and between the 2-back and 0-back ($Z = −4.78$, $p = 5.30e−6$) condition.

The median accuracy was 100% for the 0-back (IQR: [100, 100] %) and the 1-back (IQR: [95.7, 100] %) conditions, and 89.7% (IQR: [79.3, 96.6] %) for the 2-back. A significant difference was observed between the 1-back and 0-back task (Wilcoxon signed rank test, $Z = 2.60$,

p = 6.20e−3), the 2-back and 1-back (Z = 4.80, p = 5.30e−6) and between the 2-back and 0-back (Z = 4.57, p = 9.61e−6). All p-values mentioned above were corrected for multiple comparisons using false-discovery rate control (Benjamini & Hochberg, 1995).

3.2 | ERF analysis

For the 0-back condition, we observed significant activation (at least two linked voxels or timepoints) in six regions: left and medial cerebellum (80–88 ms, p_{min} = .012), precuneus (140–144 ms, p_{min} = .042), right inferior temporal gyrus (352–412 ms, p_{min} = .0001), left occipital fusiform and parahippocampal gyrus (364–380 + 412–436 ms,

p_{min} = .011), left inferior temporal gyrus (376–400 + 420–436 ms, p_{min} = .022), and left SMN (SMN; 400–436 + 460–480 + 484–496 + 508–516 ms, p_{min} = .006). With p_{min} we report the p-value for the voxel of maximum effect, or the minimum p-value found around the local maximum. See Figure 2 for the extracted ERFs and spatial distribution of the t-statistics for the 0-back condition.

Significant voxels for the 1-back condition were found in eight regions: left cerebellum (144–152 ms, p_{min} = .011), precuneus (172–188 ms, p_{min} = .002), left lateral occipital cortex (216–232 ms, p_{min} = .004), right SMN (232–256 ms, p_{min} = .008), right inferior temporal and parahippocampal gyrus (316–380 + 400–412 ms, p_{min} = .002), left inferior temporal gyrus (340–374 ms, p_{min} = .009), right middle

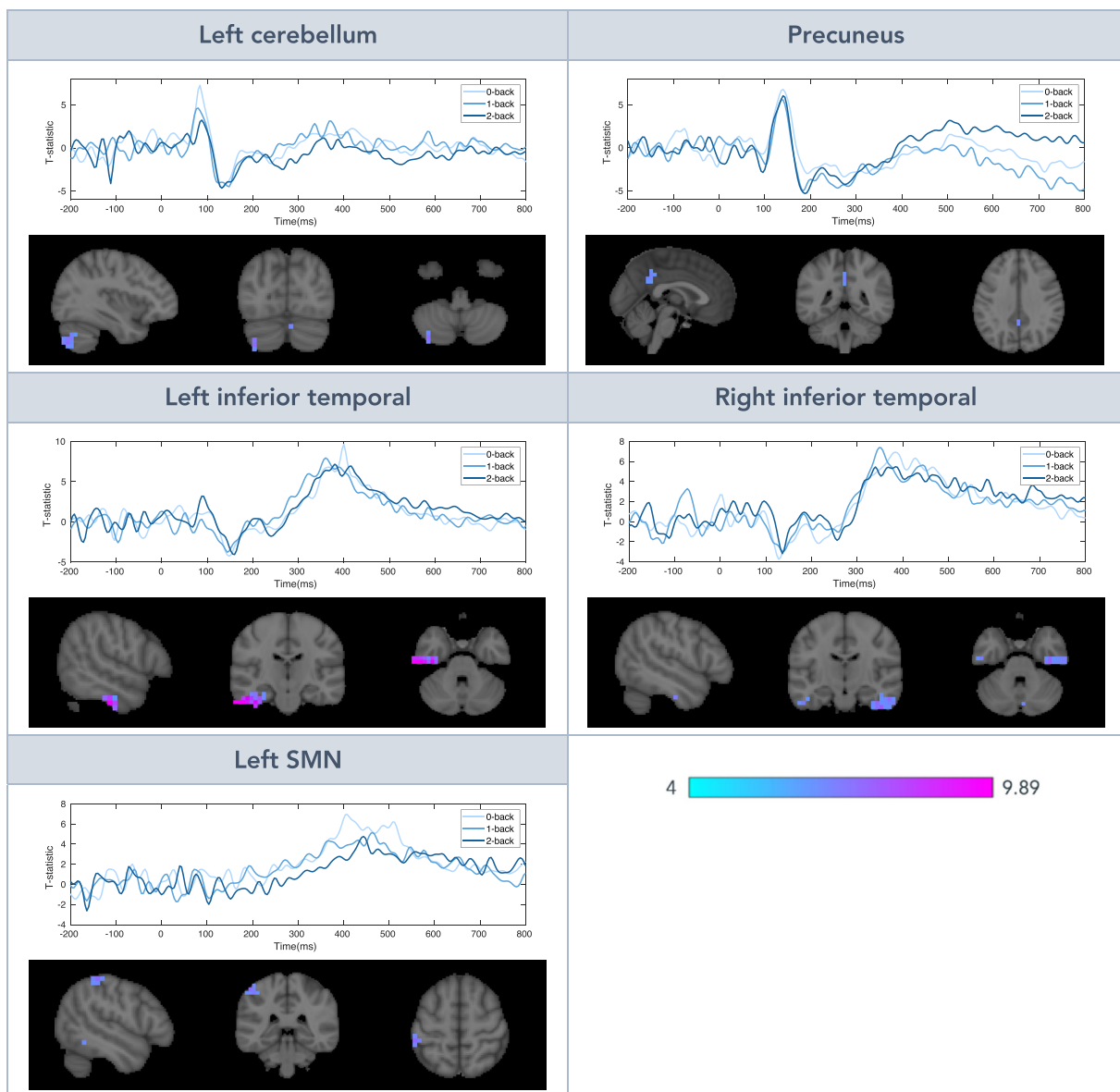**FIGURE 2** Summary of ERFs which displays the spatial distribution of five regions that were found in at least two n-back conditions. Top: ERFs for the three conditions extracted from the maximum statistic voxel for the 0-back condition. Bottom: t-statistics of the significant voxels (p < .05) for the 0-back condition at the timepoint of maximum effect. ERF, event-related field; SMN, sensorimotor network

temporal gyrus (396–420 ms, p_{min} = .004), and left SMN (432–440 + 460–472 ms, p_{min} = .014).

The 2-back condition showed significant activation in six regions, the right cerebellum (144–160 ms, p_{min} = .018), precuneus (172–192 ms, p_{min} = .003), middle SMN (244–260 ms, p_{min} = .024), left SMN (324–340 ms, p_{min} = .001), right inferior temporal and parahippocampal gyrus (324–444 + 456–472 ms, p_{min} = .0001), right temporo-occipital inferior temporal gyrus (364–464 + 516–544 + 556–576 ms, p_{min} = .002).
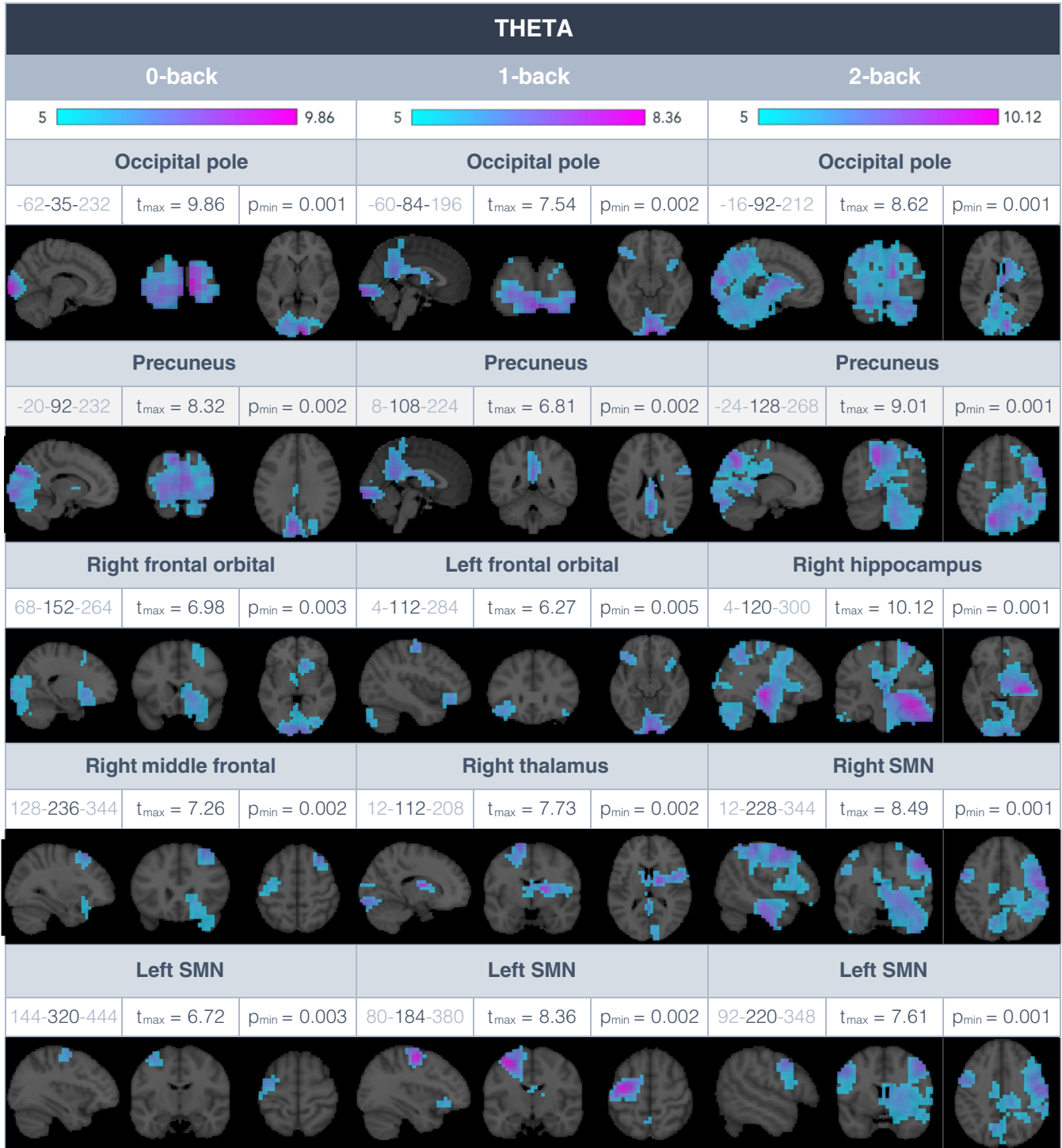
THETA

0-back			1-back			2-back		
5 — 9.86			5 — 8.36			5 — 10.12		
Occipital pole			**Occipital pole**			**Occipital pole**		
-62-35-232	t_{max} = 9.86	p_{min} = 0.001	-60-84-196	t_{max} = 7.54	p_{min} = 0.002	-16-92-212	t_{max} = 8.62	p_{min} = 0.001
Precuneus			**Precuneus**			**Precuneus**		
-20-92-232	t_{max} = 8.32	p_{min} = 0.002	8-108-224	t_{max} = 6.81	p_{min} = 0.002	-24-128-268	t_{max} = 9.01	p_{min} = 0.001
Right frontal orbital			**Left frontal orbital**			**Right hippocampus**		
68-152-264	t_{max} = 6.98	p_{min} = 0.003	4-112-284	t_{max} = 6.27	p_{min} = 0.005	4-120-300	t_{max} = 10.12	p_{min} = 0.001
Right middle frontal			**Right thalamus**			**Right SMN**		
128-236-344	t_{max} = 7.26	p_{min} = 0.002	12-112-208	t_{max} = 7.73	p_{min} = 0.002	12-228-344	t_{max} = 8.49	p_{min} = 0.001
Left SMN			**Left SMN**			**Left SMN**		
144-320-444	t_{max} = 6.72	p_{min} = 0.003	80-184-380	t_{max} = 8.36	p_{min} = 0.002	92-220-348	t_{max} = 7.61	p_{min} = 0.001

FIGURE 3 Displays the local maxima found in the t-statistic maps for the three n-back conditions in the theta band. T-stat maps are thresholded using corrected p-values (alpha = .05) resulting from MaxT permutation tests. The images along the three anatomical planes were taken at the timepoint of the maximum t-statistic. Below the anatomical region labels of the local maxima we display the timing of the effects (left), maximum t-statistic in the region over time (middle), and its corresponding p-value (right). The timing (from left to right) consists of the first timepoint where significant voxels were found in this region (light blue), the timepoint of maximum effect (dark blue), and the last timepoint with significant voxels in this region (light blue), all expressed in ms poststimulus. SMN, sensorimotor network

We found no significant differences in ERFs between the three *n*-back conditions, or effects of WM load.

3.3 | Time-frequency analysis

3.3.1 | Theta band

In Figure 3, we describe the results of the MaxT permutation tests for changes in theta power relative to baseline. In order to get a sense of the main sources of theta power changes, we focused on finding local spatiotemporal maxima of *t*-statistics. We denote the timing and *t*-value of the corresponding local maxima as $time_{max}$ and t_{max}, respectively. We observed a widespread increase in theta power with local maxima for the 0-back in the occipital pole from −62 to 232 ms ($time_{max}$ = 35 ms, t_{max} = 9.86, p_{min} = .001), precuneus from −20 until 232 ms ($time_{max}$ = 92 ms, t_{max} = 8.32, p_{min} = .002), right frontal orbital from 68 to 264 ms ($time_{max}$ = 152 ms, t_{max} = 6.98, p_{min} = .003), right middle frontal from 128 to 344 ms ($time_{max}$ = 236 ms, t_{max} = 7.26, p_{min} = .002), and left SMN from 144 to 444 ms ($time_{max}$ = 320 ms, t_{max} = 9.86, p_{min} = .001; see Figure 3, left panel). For the 1-back, local maxima were found in the occipital pole from −60 to 196 ms ($time_{max}$ = 84 ms, t_{max} = 7.54, p_{min} = .002), precuneus from 8 to 224 ms ($time_{max}$ = 108 ms, t_{max} = 6.81, p_{min} = .002), left frontal orbital from 4 to 284 ms ($time_{max}$ = 112 ms, t_{max} = 6.27, p_{min} = .005), right thalamus from 12 to 208 ms ($time_{max}$ = 112 ms, t_{max} = 7.73, p_{min} = .002), and left SMN from 80 to 380 ms ($time_{max}$ = 184 ms, t_{max} = 8.36, p_{min} = .002; see Figure 3, middle panel). Local maxima in the 2-back were the occipital pole from −16 to 212 ms ($time_{max}$ = 92 ms, t_{max} = 8.62, p_{min} = .001), precuneus from −24 to 268 ms ($time_{max}$ = 128 ms, t_{max} = 9.01, p_{min} = .001), right hippocampus from 4 to 300 ms ($time_{max}$ = 120 ms, t_{max} = 10.13, p_{min} = .001), right SMN from 12 to 344 ms ($time_{max}$ = 228 ms, t_{max} = 8.49, p_{min} = .001), and left SMN from 92 to 348 ms ($time_{max}$ = 220 ms, t_{max} = 7.61, p_{min} = .001; see Figure 3, right panel).

We found a WM load effect (2-back vs. 0-back) in the right inferior temporal gyrus from 164 to 312 ms ($time_{max}$ = 232 ms, t_{max} = 6.26, p_{min} = .016; see Figure 4). This effect is located inside the larger group of voxels showing a significant theta increase in the 2-back relative to prestimulus baseline, with a local maximum in the right hippocampus (see Figure 3, right panel).

3.3.2 | Alpha band

We observed a widespread decrease in alpha power relative to baseline. For the 0-back condition, local maxima were found in the right temporal occipital fusiform from 216 to 684 ms ($time_{max}$ = 436 ms, t_{max} = 13.51, p_{min} = .001), left occipital fusiform from 248 to 668 ms ($time_{max}$ = 468 ms, t_{max} = 12.85, p_{min} = .001), left hippocampus/inferior temporal gyrus from 280 to 668 ms ($time_{max}$ = 456 ms, t_{max} = 11.26, p_{min} = .001), and left SMN from 324 to 696 ms ($time_{max}$ = 427 ms, t_{max} = 11.11, p_{min} = .001; see Figure 5, left panel). In the 1-back, local

Theta 2 vs 0-back

6   6.26

Right inferior temporal gyrus

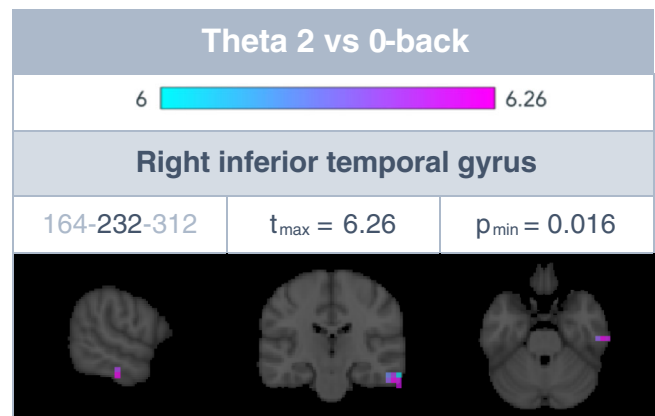| 164-**232**-312 | t_{max} = 6.26 | p_{min} = 0.016 |

FIGURE 4 Difference between the 2 and 0-back in theta power. T-stat maps are thresholded using *p*-values (alpha = .05) resulting from MaxT permutation tests. Images were taken at the timepoint of maximum *t*-statistic. Below the anatomical region labels of the local maximum we display the timing of the effects (left), maximum *t*-statistic in the region over time (middle), and its corresponding *p*-value (right). The timing (from left to right) consists of the first timepoint where significant voxels were found in this region (light blue), the timepoint of maximum effect (dark blue), and the last timepoint with significant voxels in this region (light blue)

maxima were found in the right temporal occipital fusiform from 244 to 672 ms ($time_{max}$ = 432 ms, t_{max} = 11.36, p_{min} = .001), left occipital fusiform from 252 to 676 ms ($time_{max}$ = 444 ms, t_{max} = 10.24, p_{min} = .001), left hippocampus from 260 to 672 ms ($time_{max}$ = 452 ms, t_{max} = 10.92, p_{min} = .001), and right SMN from 324 to 800 ms ($time_{max}$ = 528 ms, t_{max} = 10.75, p_{min} = .001; see Figure 5, middle panel). For the 2-back condition, the following regions contained local maxima: right temporal occipital fusiform/temporo-occipital middle temporal gyrus from 268 to 800 ms ($time_{max}$ = 404 ms, t_{max} = 10.76, p_{min} = .001), right hippocampus from 288 to 800 ms ($time_{max}$ = 496 ms, t_{max} = 12.01, p_{min} = .001), left superior parietal from 396 to 700 ms ($time_{max}$ = 512 ms, t_{max} = 11.26, p_{min} = .001), and right thalamus from 320 to 800 ms ($time_{max}$ = 596 ms, t_{max} = 12.86, p_{min} = .001; see Figure 5, right panel).

We observed a WM load effect (2-back > 0-back) on the alpha power decrease in the right occipital pole from 312 to 372 ms ($time_{max}$ = 340 ms, t_{max} = 5.96, p_{min} = .031; see Figure 6). This means that the alpha power decrease during the 2-back condition was significantly less strong than during the 0-back condition.

3.3.3 | Beta band

As for the alpha band, we observed a strong widespread decrease of beta power relative to baseline. In the 0-back condition results showed a power decrease in the left occipital fusiform from 180 to 604 ms ($time_{max}$ = 334 ms, t_{max} = 12.70, p_{min} = .001), right temporal occipital fusiform from 212 to 600 ms ($time_{max}$ = 336 ms, t_{max} = 12.96, p_{min} = .001), precuneus from 204 to 576 ms ($time_{max}$ = 376 ms, t_{max} = 12.88, p_{min} = .001), left SMN from 196 to 752 ms ($time_{max}$ = 556 ms, t_{max} = 15.16, p_{min} = .001), and right SMN from
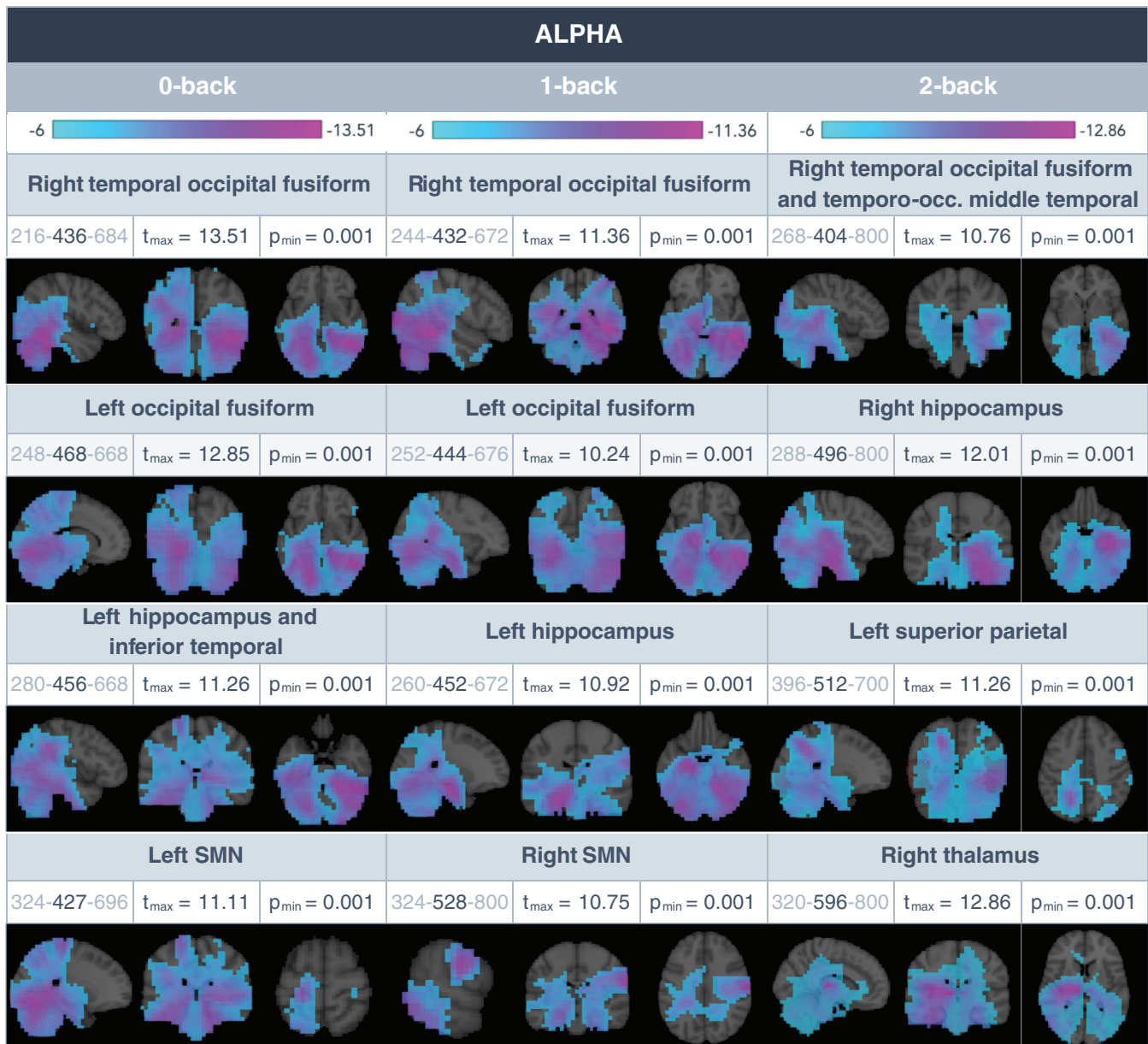
FIGURE 5 Displays the local maxima found in the *t*-statistic maps for the three *n*-back conditions in the alpha band. T-stat maps are thresholded using corrected *p*-values (alpha = .001) resulting from MaxT permutation tests. The images along the three anatomical planes were taken at the timepoint of maximum *t*-statistic. Below the anatomical region labels we display the timing of the effects (left), maximum *t*-statistic in the region over time (middle), and its corresponding *p*-value (right). The timing (from left to right) consists of the first timepoint where significant voxels were found in this region (light blue), the timepoint of maximum effect (dark blue), and the last timepoint with significant voxels in this region (light blue). SMN, sensorimotor network

220 to 744 ms (time$_{max}$ = 564 ms, t_{max} = 12.92, p_{min} = .001; see Figure 7, left panel). The 1-back condition showed local maxima in the left occipital fusiform from 176 to 608 ms (time$_{max}$ = 280 ms, t_{max} = 13.67, p_{min} = .001), right anterior supramarginal from 196 to 756 ms (time$_{max}$ = 320 ms, t_{max} = 13.08, p_{min} = .001), right temporal occipital fusiform from 200 to 584 ms (time$_{max}$ = 352 ms, t_{max} = 14.62, p_{min} = .001), and right SMN from 248 to 800 ms (time$_{max}$ = 496 ms, t_{max} = 11.07, p_{min} = .001; see Figure 7, middle panel). For the 2-back condition we observed local minima in the right lateral occipital from 172 to 560 ms (time$_{max}$ = 316 ms,

t_{max} = 12.02, p_{min} = .001), left intra-calcarine from 168 to 580 ms (time$_{max}$ = 424 ms, t_{max} = 12.66, p_{min} = .001), and left SMN from 252 to 800 ms (time$_{max}$ = 480 ms, t_{max} = 12.82, p_{min} = .001; see Figure 7, right panel).

We observed a strongly significant WM load effect (2-back > 1-back) on beta power in the right middle temporal gyrus with a maximum from 320 to 396 ms (time$_{max}$ = 348 ms, t_{max} = 8.02, p_{min} = .001; see Figure 8). This means that the beta power decrease during the 2-back condition was significantly less strong than during the 1-back condition.
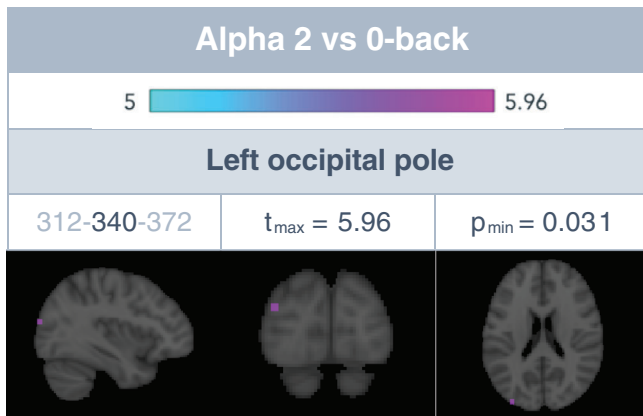
FIGURE 6 Difference between the 2 and 0-back in alpha power. T-stat maps are thresholded using *p*-values (alpha = .05) resulting from MaxT permutation tests. Images were taken at the timepoint of maximum *t*-statistic. Below the anatomical region labels of the local maximum we display the timing of the effects (left), maximum t-statistic in the region over time (middle), and its corresponding *p*-value (right). The timing (from left to right) consists of the first timepoint where significant voxels were found in this region (light blue), the timepoint of maximum effect (dark blue), and the last timepoint with significant voxels in this region (light blue)

4 | DISCUSSION

The goal of this study was to provide a full spatial, temporal, and spectral functional mapping of *n*-back multi-item WM activity, which until now contained many unclarities and inconsistencies across neuroimaging studies on the sources, temporal dynamics, and roles of ERFs and theta, alpha, and beta oscillations. In order to do this, we performed an assumption-free whole-brain analysis on verbal *n*-back MEG data. The timeline of statistically significant electrophysiological events taking place in the 0, 1, and 2-back conditions are schematically summarized in Figure 9, which we suggest the reader to use as guidance through this discussion. In the following paragraph, we provide a short summary of the main findings which will be discussed in contrast to literature in the rest of the discussion.

We identified the sources of the *n*-back M300 response in the right inferior temporal and parahippocampal gyrus and left inferior temporal gyrus, which were currently unknown. The involvement of the precuneus in *n*-back WM activity has been repeatedly shown using fMRI (Owen et al., 2005) but never using EEG or MEG, and its precise functional role is still unclear. We observed an ERF and theta power increase in the precuneus at a surprisingly early period in time, taking place between activity in brain regions responsible for lower and higher-level information processing. This suggests that the precuneus could be an important link between these two levels of information processing. As expected from literature, we observed an increase in theta power in frontal areas and were able to identify the orbitofrontal cortex as the strongest source of this effect. As previously described, the crucial role of the hippocampus during WM activity is relatively undisputable, but the ability of MEG to measure signals from the hippocampus is not. In spite of that, we found strong

evidence for an increase in theta power followed by a decrease in alpha power in the hippocampus. The latter was found to be accompanied by an almost simultaneous decrease in alpha power in the fusiform gyri, regions known to be associated with letter processing. Considering the modulatory role of alpha oscillations during WM, this suggests that these regions together enable letter recognition, encoding and storage in WM, and thus are crucial for verbal *n*-back activity.

4.1 | Event-related fields

As a novel finding, we identified the right inferior temporal and parahippocampal gyrus and left inferior temporal gyrus as sources of the *n*-back M300 ERF. This finding is consistent with studies locating an M300 in the hippocampal formation using a classic oddball task (Halgren et al., 1980; McCarthy, Wood, Williamson, & Spencer, 1989). The question then arises whether the *n*-back M300 differs from a classic stimulus matching M300. Previous scalp EEG studies reported a decrease in P300 amplitude as a consequence of increasing WM load (Covey et al., 2017; Dong et al., 2015). This effect of WM load on ERF amplitude suggests that the *n*-back M300 might not purely be a stimulus matching process. In this study, we did not observe such an effect of WM load on the amplitude of the M300 ERFs, possibly due to our conservative statistical approach, so we cannot confirm this hypothesis. Interestingly, the identified M300 sources have not been reported in *n*-back fMRI literature (see Owen et al., 2005 for an extensive meta-analysis). This is remarkable considering that neural firing in the parahippocampal gyrus has shown to correlate with the blood-oxygenated-level-dependent (BOLD) signal, which was not the case for the hippocampus (Ekstrom, 2010). A possible explanation of this discrepancy could be a mechanism that elicits an ERF but does not modulate oxygen consumption or the BOLD signal such as a phase reset. Such mechanism was described by a simultaneous fMRI-EEG study (Geukes et al., 2013), and a phase reset in a Sternberg multi-item WM task has been observed in the hippocampal system using iEEG (Kleen et al., 2016). Future studies should explore this hypothesis.

After around 85–90 ms a significant ERF was observed in the cerebellum, which was also found in the previously mentioned fMRI meta-analysis (Owen et al., 2005). While the role of the cerebellum in verbal WM has been mostly linked with an articulatory rehearsal system (Baddeley, 2003; Marvel & Desmond, 2010), this seems very unlikely when looking at its temporal occurrence. Other functions of the cerebellum during verbal WM have been claimed to be internal timing and error-driven adjustment (Ben-Yehudah, Guediche, & Fiez, 2007), the former seems a more probable explanation. This finding could however also be a consequence of visual processes and artefacts of source reconstruction techniques, which do not perform optimally outside the cerebral cortex. However, we did not expect a strong visual response during the *n*-back because the task involves only small changes in luminance. In addition, fMRI studies did not report findings in the visual cortex during the verbal *n*-back task (Owen et al., 2005).
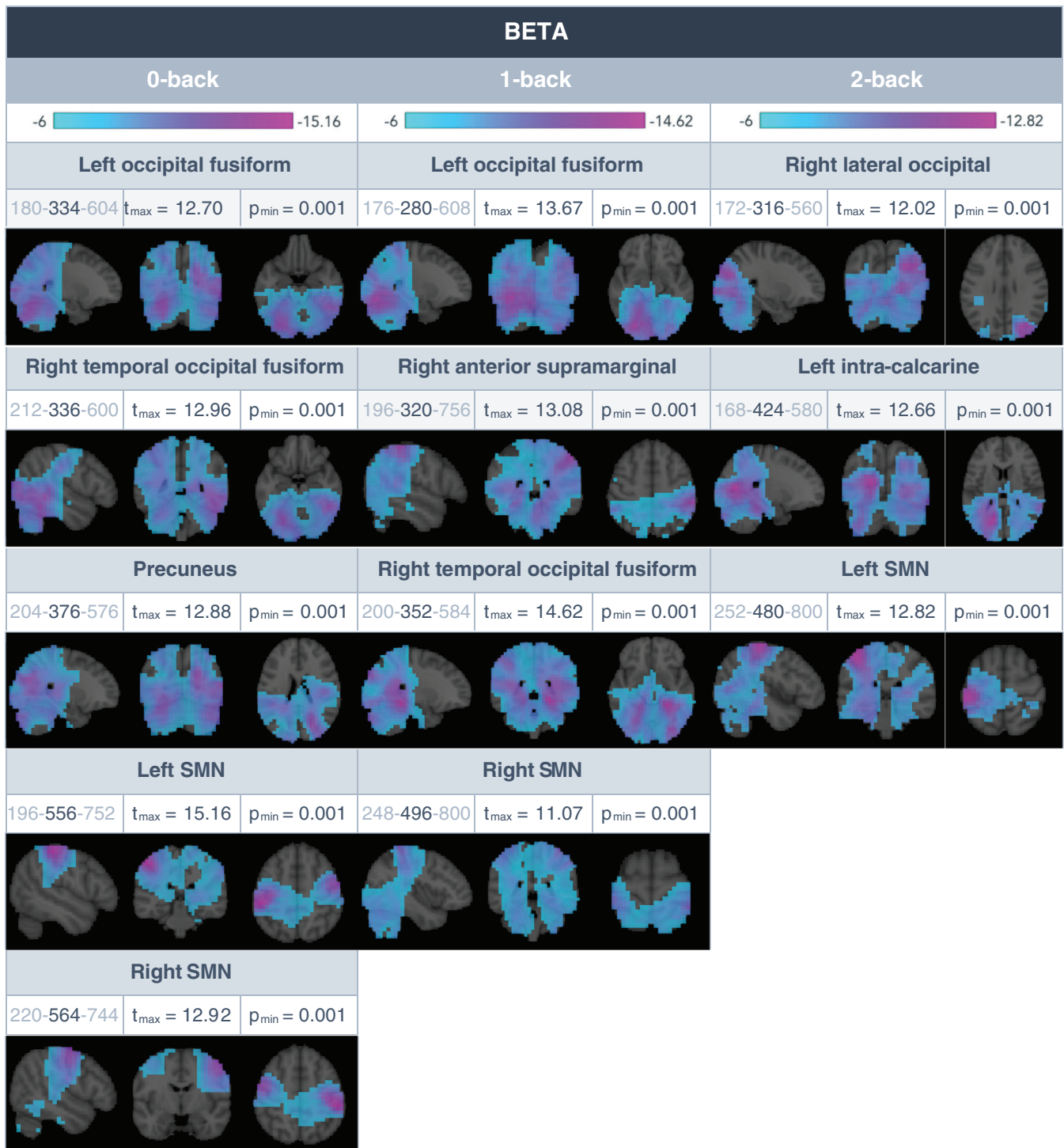
FIGURE 7 Displays the local maxima found in the *t*-statistic maps for the three *n*-back conditions in the beta band. T-stat maps are thresholded using corrected *p*-values (alpha = .001) resulting from MaxT permutation tests. The images along the three anatomical planes were taken at the timepoint of maximum *t*-statistic. Below the anatomical region labels we display the timing of the effects (left), maximum *t*-statistic in the region over time (middle), and its corresponding *p*-value (right). The timing (from left to right) consists of the first timepoint where significant voxels were found in this region (light blue), the timepoint of maximum effect (dark blue), and the last timepoint with significant voxels in this region (light blue). SMN, sensorimotor network

The precuneus also showed to be significantly activated in all *n*-back conditions around 130 ms. The precuneus has been related to spatial (Wager & Smith, 2003), episodic (Cabeza, Dolcos, Graham, & Nyberg, 2002; Fletcher et al., 1995), and (verbal) WM (Cabeza et al., 2002; Petrides, Alivisatos, Meyer, & Evans, 1993) and is consistently found in fMRI *n*-back studies (Owen et al., 2005). There is currently
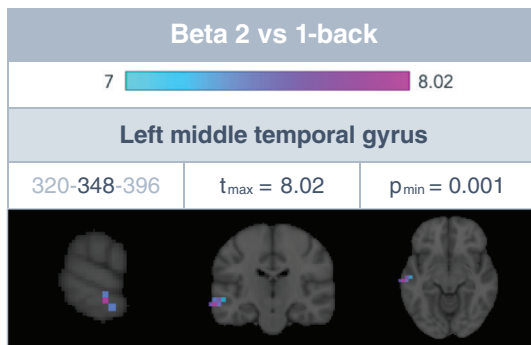
FIGURE 8 Difference between the 2 and 0-back in beta power. T-stat maps are thresholded using *p*-values (alpha = .05) resulting from MaxT permutation tests. Images were taken at the timepoint of maximum *t*-statistic. Below the anatomical region labels of the local maximum we display the timing of the effects (left), maximum *t*-statistic in the region over time (middle), and its corresponding *p*-value (right). The timing (from left to right) consists of the first timepoint where significant voxels were found in this region (light blue), the timepoint of maximum effect (dark blue), and the last timepoint with significant voxels in this region (light blue)

no clear consensus about its role but it has been suggested to mediate shifts of attention during verbal WM (Jonides et al., 1998). The precuneal ERF takes place surprisingly early and between the ERFs in the cerebellum (see Figure 9), which should reflect lower-level visual processing, and the inferior temporal lobes, which considering the observed M300 should reflect higher-level information processing.

Finally, we observed a significant increase in activity in the left SMN for the 0 and 1-back with a peak around 450 ms, strongly suggesting a motor preparation response.

4.2 | Time-frequency analysis

4.2.1 | Theta

As mentioned before, literature suggests that theta oscillations play an important role during WM for sensory processing, encoding temporal information of multiple items, and coordinating different cognitive subprocesses (Sauseng et al., 2010). We observed a strong widespread increase in theta power from around stimulus presentation to 350 ms after. The most dominant theta sources were (in that temporal order) the occipital pole, precuneus, frontal orbital cortex, right hippocampus (only for the 2-back), and left SMN (see Figure 9).

While the timing of the theta power increase in the occipital pole clearly suggests it reflects visual information processing, the timing of the power increase in the precuneus is more peculiar. Like the ERF around 130 ms, the theta power increase in the precuneus took place early at approximately 100 ms. As discussed in previous studies, theta and delta power dynamics could reflect ERF processes (Başar, Başar-Eroglu, Karakaş, & Schürmann, 2001; Demiralp, Ademoglu, Comerchero, & Polich, 2001). This hypothesis seems probable for the theta power increase and ERF in the precuneus but does not seem to

extend for ERFs reported in other brain regions. Interestingly, the precuneal theta power increase takes place after low-level visual processing in the occipital pole and an increase in theta power in the hippocampus which, as we will argue later, supposedly reflects higher-level WM encoding (see Figure 9). A study by Wallentin, Weed, Østergaard, Mouridsen, and Roepstorff (2008) found that the precuneus was the most prominent brain region in a shared network for language processing and WM. Considering this, the precuneus might function as a bridge between lower-level (visual) information and higher-level WM encoding.

An increase in frontal theta power has also been very consistently found during WM behavior (Dong et al., 2015; Gevins et al., 1997; Jensen & Tesche, 2002; Pesonen et al., 2007). In two recent studies, frontal theta power has been related to the manipulation of WM activity. One study described higher levels of frontal theta activity during manipulation processes than during WM retention processes (Griesmayr, Gruber, Klimesch, & Sauseng, 2010). A different study controlled the success of WM information manipulation by varying the difficulty of a task, which influenced theta power over the frontal cortex (Itthipuripat, Wessel, & Aron, 2013). In the current study, we observed increases in theta power in the frontal cortex during the 0 and 1-back condition around 100–250 ms after stimulus presentation. This timing could agree with the idea that frontal theta power reflects WM manipulation. In contrast to multiple studies (Brookes et al., 2011; Jensen & Tesche, 2002; Kawasaki et al., 2010; Proskovec, Heinrichs-Graham, & Wilson, 2019), we did not find an increase of frontal theta power with increasing WM load. One possible explanation could be our conservative statistical approach which could prevent us from picking up small effects. Interestingly, we were able to identify sources of the increase in frontal theta power, which were currently still ill-defined, to be the left and right orbitofrontal cortices and the right middle frontal cortex.

As described before, the role of hippocampal theta oscillations in WM encoding has been the subject of multiple studies and theories. While the measurability of the hippocampus using MEG has been the topic of debate, recent studies have shown that it is possible under some conditions (Meyer et al., 2017; Pizzo et al., 2019; Pu et al., 2018; Ruzich, Crespo-García, Dalal, & Schneiderman, 2019). For example, the minimization of coregistration errors showed to be an important factor to increase the measurability of the hippocampus, even more important than the signal-to-noise ratio (Meyer et al., 2017). In this study, we found strong evidence for an increase of theta power in the right hippocampus around 120 ms, albeit only in the 2-back condition. Additionally, we found a significant load effect on theta power (2-back > 0-back) in voxels in close proximity to the local maxima in the right hippocampus, during the second half of the time period during which voxels were found in that region. This supports the idea that the hippocampus plays a crucial role in multi-item WM encoding and confirms that we can measure it using MEG.

Finally, we found a theta power increase in the left SMN around 150 to 450 ms post-stimulus, presumably reflecting a preparatory motor response.
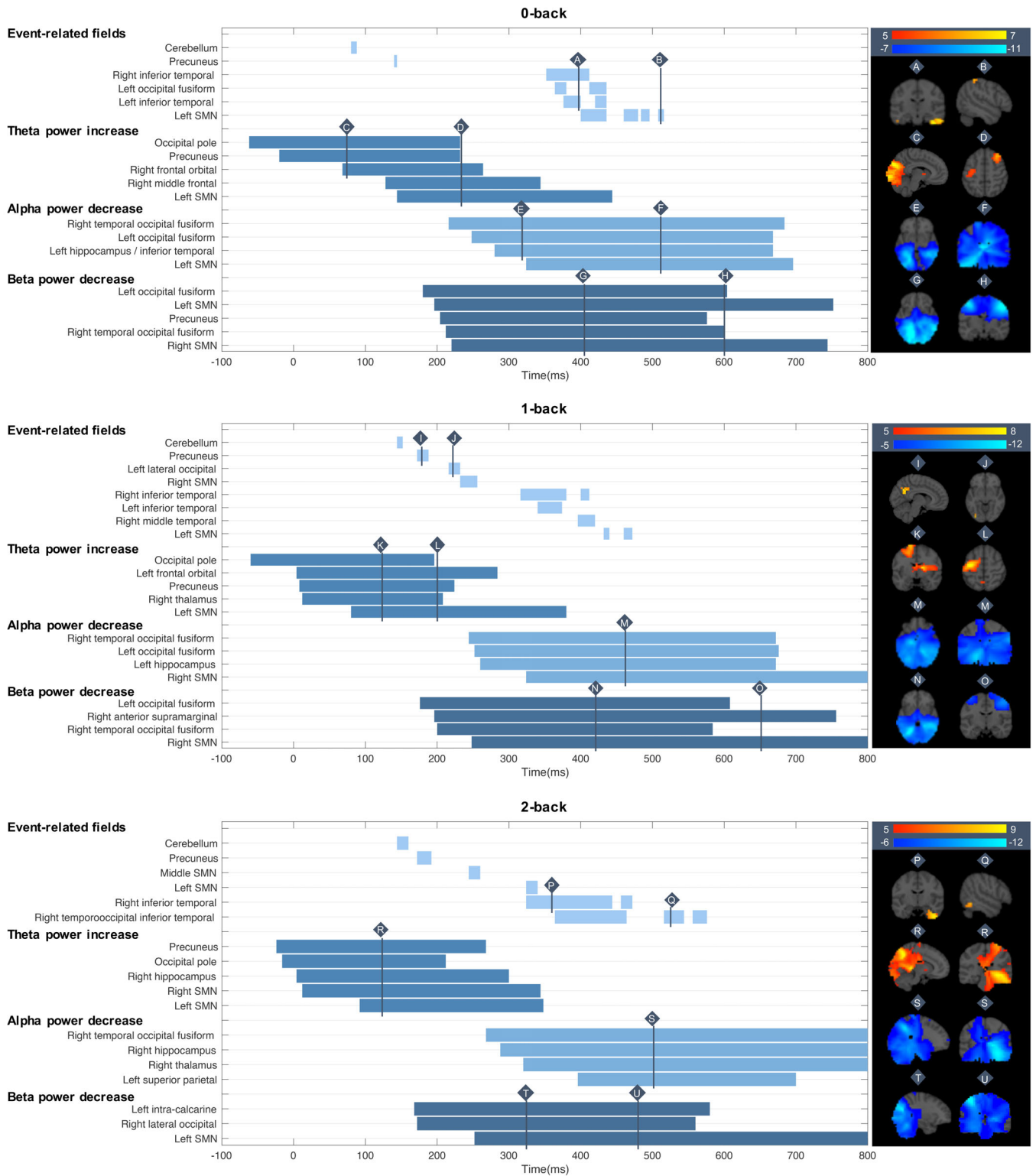
FIGURE 9 Graphic giving an overview of the results of the source space ERF and time-frequency analysis. Colored blocks display the timepoints during which a significant voxel (obtained by MaxT permutation testing over time and space) was found in a specific region. The level of statistical significance for ERF and theta time-frequency analysis was set at 0.05, while that for alpha and beta time-frequency analysis was set at 0.01. In order to give an impression of the spatial distribution of effects, source images of *t*-statistics were taken at specific timepoints and provided in the right panel. ERF, event-related field

4.2.2 | Alpha

As previously described, the role of alpha oscillations in multi-item WM has been thought to be modulatory. Increases in alpha power have shown to suppress information processing and supposedly shield WM information from distractions, while decreases in alpha power allow information processing (Haegens et al., 2011). We observed strong widespread decreases of alpha power compared to baseline from around 250 ms until 800 ms poststimulus. The main sources were the right temporal occipital fusiform, left occipital fusiform, and the left hippocampus, in that temporal order (see Figure 9). Except for the latter, these regions are in accordance with previous studies which reported posterior, parietal, and occipital sources (Roux & Uhlhaas, 2014).

The left fusiform gyrus is not a surprising finding, as it is an area which is known to be important for letter processing. Some studies have shown that the right and left fusiform sustain access to letter representations in memory (James, James, Jobard, Wong, & Gauthier, 2005; Joseph, Gathers, & Piper, 2003; Pernet, Celsis, & Démonet, 2005). Another study showed that the fusiform also couples visual form information and higher-order stimulus characteristics, which explains why the fusiform gyrus is also found to be activated during nonletter object recognition (Devlin, Jamison, Gonnerman, & Matthews, 2006). We thus suggest that the decrease in alpha power allows these processes necessary for letter processing and WM storage takes place in the fusiform gyri.

The processing of higher-order stimulus characteristics and WM encoding has been related to the hippocampus (Crottaz-Herbette, Lau, Glover, & Menon, 2005), where we similarly found a decrease in alpha power around 15–30 ms later than the alpha power decrease in the fusiform gyrus (see Figure 9). It thus seems plausible that the alpha power decrease in the fusiform gyri and left hippocampus together enables letter processing, recognition, encoding, and WM storage.

We also found a WM load effect in the occipital pole, with the alpha power decrease in the 2-back being weaker than in the 0-back. This WM load effect was located in close proximity to the local maximum in the left occipital fusiform gyrus, implying that the processes taking place in that region are modulated by the number of items in WM. This seems to suggest that the left occipital fusiform gyrus is also involved in WM encoding and storage rather than only letter processing. Future studies should investigate the interactions between the hippocampus and the occipital fusiform gyrus to learn more about the mechanisms of verbal n-back WM.

4.2.3 | Beta

It is currently unclear whether beta oscillations have a different function than alpha oscillations during WM (Roux & Uhlhaas, 2014). As mentioned before, power changes due to WM mostly spread over both alpha and beta frequency bands which led researchers to treat them as one frequency band. We found a strong decrease in beta power from around 180 to 800 ms poststimulus with the left occipital fusiform gyrus and left and right SMN as the main sources (see Figure 9).

The beta power decrease in the left occipital fusiform gyrus encompasses approximately the same timing as the alpha power decrease in the same region. Considering its role in letter processing, this seems to suggest that indeed alpha and beta frequency oscillations have the same function during WM behavior, at least in that region, namely a modulatory function through inhibition and disinhibition.

The beta power decrease in the left and right SMN had a maximum effect around the median response time. Beta desynchronization in the SMN during movement preparation has been repeatedly reported (Pfurtscheller, 1989; Salenius & Hari, 2003; Zhang, Chen, Bressler, & Ding, 2008). These power changes picked up by MEG in the SMN are thought to arise through the firing of excitatory pyramidal cells (Jensen et al., 2005).

We also found a WM load effect in the middle temporal gyrus, with the beta power decrease in the 2-back being less strong than in the 0-back. This effect was not located near a local maximum in one of the n-back conditions and is therefore difficult to interpret.

5 | CONCLUSION

In conclusion, this study provides an elaborate whole-brain enquiry into n-back verbal WM activity. We shed new light on the role and dynamics of ERFs and theta, alpha, and beta oscillatory changes while illustrating the important role of regions such as the precuneus, hippocampus, orbitofrontal cortex, and occipital fusiform gyrus during verbal n-back WM.

6 | LIMITATIONS

While using the n-back task rather than the DMS task for studying WM has certain advantages such as a more consistent theta power increase (Brookes et al., 2011), it is impossible to isolate specific WM processes such as WM maintenance, which is possible using the DMS task. This limits the conclusions that can be made about the involvement of brain regions in specific processes.

CONFLICT OF INTEREST

The authors report no competing interests.

DATA AVAILABILITY STATEMENT

The data for this study are not publicly available. Researchers interested in a collaboration on these data are welcome to contact the senior authors. Analysis scripts are available upon request from the corresponding author.

ORCID

Lars Costers https://orcid.org/0000-0003-2668-8061

Jeroen Van Schependom https://orcid.org/0000-0003-1200-5872

Jorne Laton https://orcid.org/0000-0003-4215-6524

Johan Baijot https://orcid.org/0000-0003-1108-7845

Martin Sjøgård https://orcid.org/0000-0002-7768-9454

Xavier De Tiège https://orcid.org/0000-0003-0127-089X

Serge Goldman https://orcid.org/0000-0002-9917-8735

Marie Beatrice D'hooghe https://orcid.org/0000-0002-0917-4176

Guy Nagels https://orcid.org/0000-0002-2597-0383

REFERENCES

Axmacher, N., Henseler, M. M., Jensen, O., Weinreich, I., Elger, C. E., & Fell, J. (2010). Cross-frequency coupling supports multi-item working memory in the human hippocampus. *Proceedings of the National Academy of Sciences of the United States of America, 107*(7), 3228–3233. https://doi.org/10.1073/pnas.0911531107

Axmacher, N., Mormann, F., Fernández, G., Cohen, M. X., Elger, C. E., & Fell, J. (2007). Sustained neural activity patterns during working memory in the human medial temporal lobe. *The Journal of Neuroscience, 27*, 7807–7816. https://doi.org/10.1523/JNEUROSCI.0962-07.2007

Baddeley, A. (2003). Working memory: Looking back and looking forward. *Nature Reviews Neuroscience., 4*, 829–839. https://doi.org/10.1038/nrn1201

Başar, E., Başar-Eroglu, C., Karakaş, S., & Schürmann, M. (2001). Gamma, alpha, delta, and theta oscillations govern cognitive processes. *International Journal of Psychophysiology, 39*(2–3), 241–248. https://doi.org/10.1016/S0167-8760(00)00145-8

Bastos, A. M., Loonis, R., Kornblith, S., Lundqvist, M., & Miller, E. K. (2018). Laminar recordings in frontal cortex suggest distinct layers for maintenance and control of working memory. *Proceedings of the National Academy of Sciences of the United States of America., 115*, 1117–1122. https://doi.org/10.1073/pnas.1710323115

Ben-Yehudah, G., Guediche, S., & Fiez, J. A. (2007). Cerebellar contributions to verbal working memory: Beyond cognitive theory. *Cerebellum, 6*, 193–201. https://doi.org/10.1080/14734220701286195

Benjamini, Y., & Hochberg, Y. (1995). Controlling the False Discovery Rate: A Practical and Powerful Approach to Multiple Testing. *Journal of the Royal Statistical Society: Series B (Methodological)., 57*, 289–300. https://doi.org/10.1111/j.2517-6161.1995.tb02031.x

Bočková, M., Chládek, J., Jurák, P., Halámek, J., & Rektor, I. (2007). Executive functions processed in the frontal and lateral temporal cortices: Intracerebral study. *Clinical Neurophysiology, 118*, 2625–2636. https://doi.org/10.1016/j.clinph.2007.07.025

Bonnefond, M., & Jensen, O. (2012). Alpha oscillations serve to protect working memory maintenance against anticipated distracters. *Current Biology, 22*(20), 1969–1974. https://doi.org/10.1016/j.cub.2012.08.029

Brookes, M. J., Wood, J. R., Stevenson, C. M., Zumer, J. M., White, T. P., Liddle, P. F., & Morris, P. G. (2011). Changes in brain network activity during working memory tasks: A magnetoencephalography study. *NeuroImage, 55*(4), 1804–1815. https://doi.org/10.1016/j.neuroimage.2010.10.074

Cabeza, R., Dolcos, F., Graham, R., & Nyberg, L. (2002). Similarities and differences in the neural correlates of episodic memory retrieval and working memory. *NeuroImage, 16*(2), 317–330. https://doi.org/10.1006/nimg.2002.1063

Chen, Y., & Huang, X. (2016). Modulation of alpha and beta oscillations during an *n*-back task with varying temporal memory load. *Frontiers in Psychology, 6*, 1–10. https://doi.org/10.3389/fpsyg.2015.02031

Covey, T. J., Shucard, J. L., & Shucard, D. W. (2017). Event-related brain potential indices of cognitive function and brain resource reallocation during working memory in patients with Multiple Sclerosis. *Clinical Neurophysiology, 128*(4), 604–621. https://doi.org/10.1016/j.clinph.2016.12.030

Crottaz-Herbette, S., Lau, K. M., Glover, G. H., & Menon, V. (2005). Hippocampal involvement in detection of deviant auditory and visual stimuli. *Hippocampus, 15*(1), 132–139. https://doi.org/10.1002/hipo.20039

De Tiège, X., de Beeck, M. O., Funke, M., Legros, B., Parkkonen, L., Goldman, S., & Van Bogaert, P. (2008). Recording epileptic activity with MEG in a light-weight magnetic shield. *Epilepsy Research, 82*(2–3), 227–231. https://doi.org/10.1016/j.eplepsyres.2008.08.011

Deiber, M. P., Missonnier, P., Bertrand, O., Gold, G., Fazio-Costa, L., Ibañez, V., & Giannakopoulos, P. (2007). Distinction between perceptual and attentional processing in working memory tasks: A study of phase-locked and induced oscillatory brain dynamics. *Journal of Cognitive Neuroscience., 19*, 158–172. https://doi.org/10.1162/jocn.2007.19.1.158

Demiralp, T., Ademoglu, A., Comerchero, M., & Polich, J. (2001). *Wavelet analysis of P3a and P3b. Brain topography, 13*(4), 251–267.

Devlin, J. T., Jamison, H. L., Gonnerman, L. M., & Matthews, P. M. (2006). The role of the posterior fusiform gyrus in reading. *Journal of Cognitive Neuroscience, 18*(6), 911–922. https://doi.org/10.1162/jocn.2006.18.6.911

Donchin, E., Ritter, W., & McCallum, W. C. (1978). Cognitive psychophysiology: The endogenous components of the ERP. *Event-Related Brain Potentials in Man, 349*, 411. https://doi.org/10.1016/b978-0-12-155150-6.50019-5

Dong, S., Reder, L. M., Yao, Y., Liu, Y., & Chen, F. (2015). Individual differences in working memory capacity are reflected in different ERP and EEG patterns to task difficulty. *Brain Research, 1616*, 146–156. https://doi.org/10.1016/j.brainres.2015.05.003

Ekstrom, A. (2010). How and when the fMRI BOLD signal relates to underlying neural activity: The danger in dissociation. *Brain Research Reviews., 62*, 233–244. https://doi.org/10.1016/j.brainresrev.2009.12.004

Fletcher, P. C., Frith, C. D., Baker, S. C., Shallice, T., Frackowiak, R. S. J., & Dolan, R. J. (1995). The mind's eye—recuneus activation in memory-related imagery. *NeuroImage, 2*(3), 195–200. https://doi.org/10.1006/nimg.1995.1025

Fortin, N. J., Agster, K. L., & Eichenbaum, H. B. (2002). Critical role of the hippocampus in memory for sequences of events. *Nature Neuroscience, 5*(5), 458–462. https://doi.org/10.1038/nn834

Geukes, S., Huster, R. J., Wollbrink, A., Junghö Fer, M., Zwitserlood, P., & Dobel, C. (2013). *A large N400 but no BOLD effect-comparing source activations of semantic priming in simultaneous EEG-fMRI. PloS one, 8*(12). Chicago.

Gevins, A., Smith, M. E., Leong, H., McEvoy, L., Whitfield, S., Du, R., & Rush, G. (1998). Monitoring working memory load during computer-based tasks with EEG pattern recognition methods. *Human Factors., 40*, 79–91. https://doi.org/10.1518/001872098779480578

Gevins, A., Smith, M. E., McEvoy, L., & Yu, D. (1997). High-resolution EEG mapping of cortical activation related to working memory: Effects of task difficulty, type of processing, and practice. *Cerebral Cortex., 7*, 374–385. https://doi.org/10.1093/cercor/7.4.374

Griesmayr, B., Gruber, W. R., Klimesch, W., & Sauseng, P. (2010). Human frontal midline theta and its synchronization to gamma during a verbal delayed match to sample task. *Neurobiology of Learning and Memory, 93*(2), 208–215. https://doi.org/10.1016/j.nlm.2009.09.013

Haegens, S., Nácher, V., Luna, R., Romo, R., & Jensen, O. (2011). α-Oscillations in the monkey sensorimotor network influence discrimination performance by rhythmical inhibition of neuronal spiking. *Proceedings of the National Academy of Sciences of the United States of America, 108*(48), 19377–19382. https://doi.org/10.1073/pnas.1117190108

Halgren, E., Squires, N. K., Wilson, C. L., Rohrbaugh, J. W., Babb, T. L., & Crandall, P. H. (1980). Endogenous potentials generated in the human hippocampal formation and amygdala by infrequent events. *Science, 210*, 803–805. https://doi.org/10.1126/science.7434000

Hari, R., & Salmelin, R. (2012, June). Magnetoencephalography: From SQUIDs to neuroscience. Neuroimage 20th Anniversary Special

Edition. *NeuroImage*, *61*(2), 386–396. https://doi.org/10.1016/j.neuroimage.2011.11.074

Hsieh, L. T., Ekstrom, A. D., & Ranganath, C. (2011). Neural oscillations associated with item and temporal order maintenance in working memory. *Journal of Neuroscience.*, *31*, 10803–10810. https://doi.org/10.1523/JNEUROSCI.0828-11.2011

Itthipuripat, S., Wessel, J. R., & Aron, A. R. (2013). Frontal theta is a signature of successful working memory manipulation. *Experimental Brain Research*, *224*(2), 255–262. https://doi.org/10.1007/s00221-012-3305-3

James, K. H., James, T. W., Jobard, G., Wong, A. C. N., & Gauthier, I. (2005). Letter processing in the visual system: Different activation patterns for single letters and strings. *Cognitive, Affective, & Behavioral Neuroscience*, *5*, 452–466. https://doi.org/10.3758/CABN.5.4.452

Jensen, O., Goel, P., Kopell, N., Pohja, M., Hari, R., & Ermentrout, B. (2005). On the human sensorimotor-cortex beta rhythm: Sources and modeling. *NeuroImage*, *26*(2), 347–355. https://doi.org/10.1016/j.neuroimage.2005.02.008

Jensen, O., & Tesche, C. D. (2002). Frontal theta activity in humans increases with memory load in a working memory task. *European Journal of Neuroscience.*, *15*, 1395–1399. https://doi.org/10.1046/j.1460-9568.2002.01975.x

Jonides, J., Schumacher, E. H., Smith, E. E., Koeppe, R. A., Awh, E., Reuter-Lorenz, P. A., … Willis, C. R. (1998). The role of parietal cortex in verbal working memory. *The Journal of Neuroscience*, *18*(13), 5026–5034. https://doi.org/10.1523/JNEUROSCI.18-13-05026.1998

Joseph, J. E., Gathers, A. D., & Piper, G. A. (2003). Shared and dissociated cortical regions for object and letter processing. *Cognitive Brain Research*, *17*(1), 56–67. https://doi.org/10.1016/S0926-6410(03)00080-6

Kawasaki, M., Kitajo, K., & Yamaguchi, Y. (2010). Dynamic links between theta executive functions and alpha storage buffers in auditory and visual working memory. *European Journal of Neuroscience*, *31*(9), 1683–1689. https://doi.org/10.1111/j.1460-9568.2010.07217.x

Kesner, R. P., Gilbert, P. E., & Barua, L. A. (2002). The role of the hippocampus in memory for the temporal order of a sequence of odors. *Behavioral Neuroscience*, *116*(2), 286–290. https://doi.org/10.1037/0735-7044.116.2.286

Kirchner, W. K. (1958). Age differences in short-term retention of rapidly changing information. *Journal of Experimental Psychology*, *55*(4), 352–358. https://doi.org/10.1037/h0043688

Kleen, J. K., Testorf, M. E., Roberts, D. W., Scott, R. C., Jobst, B. J., Holmes, G. L., & Lenck-Santini, P. P. (2016). Oscillation phase locking and late ERP components of intracranial hippocampal recordings correlate to patient performance in a working memory task. *Frontiers in Human Neuroscience*, *10*(June), 1–14. https://doi.org/10.3389/fnhum.2016.00287

Kok, A. (2001). On the utility of P3 amplitude as a measure of processing capacity. *Psychophysiology*, *38*(3), 557–577. https://doi.org/10.1017/s0048577201990559

Krause, C. M., Pesonen, M., & Hämäläinen, H. (2010). Brain oscillatory 4–30Hz electroencephalogram responses in adolescents during a visual memory task. *Neuroreport*, *21*, 767–771. https://doi.org/10.1097/WNR.0b013e32833bfcbb

Lei, S., & Roetting, M. (2011). Influence of task combination on EEG spectrum modulation for driver workload estimation. *Human Factors.*, *53*, 168–179. https://doi.org/10.1177/0018720811400601

Leszczynski, M. (2011). How does hippocampus contribute to working memory processing? *Frontiers in Human Neuroscience*, *5*, 168. https://doi.org/10.1523/jneurosci.0702-11.2011

Lisman, J. E., & Idiart, M. A. P. (1995). Storage of 7 ± 2 short-term memories in oscillatory subcycles. *Science*, *267*(5203), 1512–1515. https://doi.org/10.1126/science.7878473

Lisman, J. E., & Jensen, O. (2013, March 20). The theta-gamma neural code. *Neuron*, *77*, 1002–1016. https://doi.org/10.1016/j.neuron.2013.03.007

Marvel, C. L., & Desmond, J. E. (2010). Functional topography of the cerebellum in verbal working memory. *Neuropsychology Review*, *20*, 271–279. https://doi.org/10.1007/s11065-010-9137-7

McCarthy, G., Wood, C. C., Williamson, P. D., & Spencer, D. D. (1989). Task-dependent field potentials in human hippocampal formation. *Journal of Neuroscience*, *9*(12), 4253–4268. https://doi.org/10.1523/jneurosci.09-12-04253.1989

Meyer, S. S., Rossiter, H., Brookes, M. J., Woolrich, M. W., Bestmann, S., & Barnes, G. R. (2017). Using generative models to make probabilistic statements about hippocampal engagement in MEG. *NeuroImage*, *149* (June 2016), 468–482. https://doi.org/10.1016/j.neuroimage.2017.01.029

Nichols, T. E., & Holmes, A. P. (2002). Nonparametric permutation tests for functional neuroimaging: A primer with examples. *Human Brain Mapping.*, *15*, 1–25. https://doi.org/10.1002/hbm.1058

Nichols, T., & Holmes, A. (2003). Nonparametric permutation tests for functional neuroimaging. In *Human brain function* (2nd ed.). *25*, 887–910.

Oostenveld, R., Fries, P., Maris, E., & Schoffelen, J. M. (2011). FieldTrip: Open source software for advanced analysis of MEG, EEG, and invasive electrophysiological data. *Computational Intelligence and Neuroscience*, *2011*, 1–9. https://doi.org/10.1155/2011/156869

Owen, A. M., McMillan, K. M., Laird, A. R., & Bullmore, E. (2005). *n*-Back working memory paradigm: A meta-analysis of normative functional neuroimaging studies. *Human Brain Mapping.*, *25*, 46–59. https://doi.org/10.1002/hbm.20131

Palva, S., Kulashekhar, S., Hämäläinen, M., & Palva, J. M. (2011). Localization of cortical phase and amplitude dynamics during visual working memory encoding and retention. *Journal of Neuroscience.*, *31*, 5013–5025. https://doi.org/10.1523/JNEUROSCI.5592-10.2011

Pernet, C., Celsis, P., & Démonet, J. F. (2005). Selective response to letter categorization within the left fusiform gyrus. *NeuroImage*, *28*(3), 738–744. https://doi.org/10.1016/j.neuroimage.2005.06.046

Pesonen, M., Hämäläinen, H., & Krause, C. M. (2007). Brain oscillatory 4-30 Hz responses during a visual *n*-back memory task with varying memory load. *Brain Research*, *1138*(1), 171–177. https://doi.org/10.1016/j.brainres.2006.12.076

Petrides, M., Alivisatos, B., Meyer, E., & Evans, A. C. (1993). Functional activation of the human frontal cortex during the performance of verbal working memory tasks. *Proceedings of the National Academy of Sciences of the United States of America*, *90*, 878–882. https://doi.org/10.1073/pnas.90.3.878

Pfurtscheller, G. (1989). Functional topography during sensorimotor activation studied with event-related desynchronization mapping. *Journal of Clinical Neurophysiology*, *6*(1), 75–84. https://doi.org/10.1097/00004691-198901000-00003

Pizzo, F., Roehri, N., Medina Villalon, S., Trébuchon, A., Chen, S., Lagarde, S., … Bénar, C. G. (2019). Deep brain activities can be detected with magnetoencephalography. *Nature Communications*, *10* (1), 971. https://doi.org/10.1038/s41467-019-08665-5

Proskovec, A. L., Heinrichs-Graham, E., & Wilson, T. W. (2019). Load modulates the alpha and beta oscillatory dynamics serving verbal working memory. *NeuroImage*, *184*(September 2018), 256–265. https://doi.org/10.1016/j.neuroimage.2018.09.022

Pu, Y., Cheyne, D. O., Cornwell, B. R., & Johnson, B. W. (2018). Noninvasive investigation of human hippocampal rhythms using magnetoencephalography: A review. *Frontiers in Neuroscience*, *12*, 273. https://doi.org/10.3389/fnins.2018.00273

Raghavachari, S., Lisman, J. E., Tully, M., Madsen, J. R., Bromfield, E. B., & Kahana, M. J. (2006). Theta oscillations in human cortex during a working-memory task: Evidence for local generators. *Journal of Neurophysiology*, *95*, 1630–1638. https://doi.org/10.1152/jn.00409.2005

Raghavachari, S., Kahana, M. J., Rizzuto, D. S., Caplan, J. B., Kirschen, M. P., Bourgeois, B., … Lisman, J. E. (2001). Gating of human theta oscillations by a working memory task. *Journal of Neuroscience*, *21*(9), 3175–3183.

Roberts, B. M., Hsieh, L. T., & Ranganath, C. (2013). Oscillatory activity during maintenance of spatial and temporal information in working memory. *Neuropsychologia*, *51*, 349–357. https://doi.org/10.1016/j.neuropsychologia.2012.10.009

Rosner, B. (1983). Percentage points for a generalized ESD many-outlier procedure. *Technometrics*, *25*(2), 165. https://doi.org/10.2307/1268549

Roux, F., & Uhlhaas, P. J. (2014). Working memory and neural oscillations: Alpha-gamma versus theta-gamma codes for distinct WM information? *Trends in Cognitive Sciences*, *18*(1), 16–25. https://doi.org/10.1016/j.tics.2013.10.010

Ruzich, E., Crespo-García, M., Dalal, S. S., & Schneiderman, J. F. (2019). Characterizing hippocampal dynamics with MEG: A systematic review and evidence-based guidelines. *Human Brain Mapping*, *40*(4), 1353-1375.

Salenius, S., & Hari, R. (2003). Synchronous cortical oscillatory activity during motor action. *Current Opinion in Neurobiology*, *13*, 678–684. https://doi.org/10.1016/j.conb.2003.10.008

Sauseng, P., Griesmayr, B., Freunberger, R., & Klimesch, W. (2010). Control mechanisms in working memory: A possible function of EEG theta oscillations. *Neuroscience and Biobehavioral Reviews*, *34*(7), 1015–1022. https://doi.org/10.1016/j.neubiorev.2009.12.006

Tallon-Baudry, C., Bertrand, O., Peronnet, F., & Pernier, J. (1998). Induced gamma-band activity during the delay of a visual short-term memory task in humans. *Journal of Neuroscience*, *18*(11), 4244–4254. https://doi.org/10.1523/jneurosci.18-11-04244.1998

Van Vugt, M. K., Schulze-Bonhage, A., Litt, B., Brandt, A., & Kahana, M. J. (2010). Hippocampal gamma oscillations increase with memory load. *Journal of Neuroscience.*, *30*, 2694–2699. https://doi.org/10.1523/JNEUROSCI.0567-09.2010

Wager, T. D., & Smith, E. E. (2003). Neuroimaging studies of working memory. *Cognitive, Affective, & Behavioral Neuroscience*, *3*(4), 255-274.

Wallentin, M., Weed, E., Østergaard, L., Mouridsen, K., & Roepstorff, A. (2008). Accessing the mental space—Spatial working memory processes for language and vision overlap in precuneus. *Human Brain Mapping.*, *29*, 524–532. https://doi.org/10.1002/hbm.20413

Woolrich, M., Hunt, L., Groves, A., & Barnes, G. (2011). MEG beamforming using Bayesian PCA for adaptive data covariance matrix regularization. *NeuroImage*, *57*(4), 1466–1479. https://doi.org/10.1016/j.neuroimage.2011.04.041

Zhang, Y., Chen, Y., Bressler, S. L., & Ding, M. (2008). Response preparation and inhibition: The role of the cortical sensorimotor beta rhythm. *Neuroscience*, *156*(1), 238–246. https://doi.org/10.1016/j.neuroscience.2008.06.061